Supporting Information

A Fe single atom on N,S-doped carbon catalyst performing *N*-Alkylation of Aromatic Amines under Solvent-free Conditions

Guo-Ping Lu[+*a] , *Hongbin Shan*[+a], *Yamei Lin*[b], *Kai Zhang*[a], *Baojing Zhou*[a], *Qin Zhong*[a], *Pengcheng Wang**[a]

[a] School of Chemistry and Chemical Engineering, Nanjing University of Science & Technology, Xiaolingwei 200, Nanjing 210094, P. R. China.

[b] School of Food Science and Pharmaceutical Engineering, Nanjing Normal University, Wenyuanstreet 200, Nanjing 210032, China.

Characterization

All chemical reagents are obtained from commercial suppliers and used without further purification. GC-MS analyses are performed on an ISQ Trace 1300 in the electron ionization (EI) mode. GC analyses are performed on an Agilent 7890A instrument (Column: Agilent 19091J413: 30 m × 320 μm × 0.25 μm, carrier gas: H_2, FID detection. XRD analysis was performed on a Shimadzu X-ray diffractometer (XRD-6000) with Cu K_α irradiation. The transmission electron microscopy (TEM) images were recorded using a PHILIPS Tecnai 12 microscope operating at 120 kV. X-ray photoelectron spectroscopy (XPS) was performed on an ESCALAB 250Xi spectrometer, using an Al Kα X-ray source (1486.6 eV of photons) and calibrated by setting the C 1s peak to 284.80 eV. Inductively coupled plasma mass spectrometry (ICP-MS) was analyzed on an Optima 7300 DV. The BET surface area and pore size measurements were performed with N_2 adsorption/desorption isotherms at 77 K on a Micromeritics ASAP 2020 instrument. Before measurements, the samples were degassed at 80 °C for 12 h. The X-ray absorption fine structure (XAFS) spectra (Fe K-edge) were collected at BL14W beamline in Shanghai Synchrotron Radiation Facility (SSRF). The storage rings of SSRF was operated at 3.5 GeV with a stable current of 200 mA. Using Si(111) double-crystal monochromator, the data collection were carried out in fluorescence mode using Lytle detector. All spectra were collected in ambient conditions. The HAADF-STEM and EDX-mapping analysis were performed on Titan ETEM Themis. The IR images were recorded using a NICOLETIS10. The Raman analysis was performed on horiba evolution.

Catalysts preparation

The synthesis of Fe@NSCs and Fe_{20}-SA@NC

First, 32 mmol 2-MeIm and 32 mmol aniline were dissolved in 80 mL deionized water. Meanwhile, 8 mmol $Zn(NO_3)_2{\cdot}6H_2O$ and 0.4 mmol $FeSO_4{\cdot}7H_2O$ were dissolved in 80 mL deionized water by sonication for 10 min. The obtained salt solution was added to the above 2-MeIm and aniline solution under vigorous stirring at room temperature for 12 h. The obtained sample was centrifuged and washed with

deionized water. The final product Fe_{20}-ZIF-8@PAN was dried under vacuum at 60 °C for 12 h. By changing the amount of $FeSO_4 \cdot 7H_2O$, the precursor Fe_{10}-ZIF-8@PAN and Fe_{40}-ZIF-8@PAN (the number represent the molar ration of $Zn(NO_3)_2 \cdot 6H_2O$ and $FeSO_4 \cdot 7H_2O$) were prepared. Subsequently, the prepared precursor was treated at 900 ℃ under N_2 atmosphere for 2 h to obtain carbon-based catalyst. The Fe_{10}-ZIF-8@PAN, Fe_{20}-ZIF-8@PAN and Fe_{40}-ZIF-8@PAN were transformed to Fe_{10}-NP@NSC and Fe_{20}-SA@NSC and Fe_{40}-SA@NSC, respectively. (The NP represent nanoparticle catalyst and the SA represent single-atom catalyst).

The synthesis steps of Fe_{20}-SA@NC are the same with Fe_{20}-SA@NSC, except that $Fe(NO_3)_3 \cdot 9H_2O$ is used instead of $FeSO_4 \cdot 7H_2O$.

The synthesis of NC

First, 32 mmol 2-MeIm was dissolved in 80 mL deionized water. Meanwhile, 8 mmol $Zn(NO_3)_2 \cdot 6H_2O$ was dissolved in 80 mL deionized water by sonication for 10 min. The obtained salt solution was added to the above 2-MeIm solution under vigorous stirring at room temperature for 12 h. The obtained sample was centrifuged and washed with deionized water. The final product ZIF-8 was dried under vacuum at 60 °C for 12 h. Subsequently, the prepared ZIF-8 was treated at 900 ℃ under N_2 atmosphere for 2 h to obtain the catalyst NC.

The synthesis of Fe@C

The 200 mg lignin, 100 mg $ZnCl_2$ and 50 mg $FeCl_3$ were dissolved in 80 mL ethanol. After stirring for 4 h at room temperature, the obtained sample was collected by centrifugation. Subsequently, the prepared sample was treated at 900 ℃ under N_2 atmosphere for 2 h to obtain the catalyst Fe@C.

Catalytic reaction

In a typical reaction procedure, 3 mmol aniline, 6 mmol benzyl alcohol, 0.9 mmol KOH and 20 mg of Fe_{20}-SA@NSC (0.3 mol% of Fe) were placed in a 25 mL sealed tube, and then the tube was purged with Ar gas. The reaction mixture was heated at 135 ℃ for 24 h. After the reaction completed, the sealed tube was cooled down to room temperature, and the solution was diluted by ethyl acetate and analyzed by gas

chromatography (GC) and GC-mass spectroscopy (GC-MS).

Recyclability test

In order to investigate the recyclability of Fe_{20}-SA@NSC, the catalyst was collected by centrifugation after the reaction was completed, washed by ethyl acetate and directly reused for next reaction cycle.

DFT Calculations

The structural models for the catalysts were constructed by replacing five C atoms in the graphene fragment with four N atoms and one Fe atom. For Fe_1-N_4S_1, Fe_1-N_4O_1 and Fe_1-N_5, the -S-CH_3, -O-CH_3, -NH-CH_3 groups are coordinated to the Fe atom from below, respectively. Finally, the C atoms on the edge of the graphene fragment are saturated with H atoms. After the substrate is adsorbed on the Fe atom from above, the three reactant structures are obtained. The three product structures were constructed in a similar way. These six structures were optimized at the B3LYP level using the Gaussian09 program.[1] The 6-31G(d) basis set and LANL2DZ effective core potential basis set[2][3] were employed for the light atoms Fe atom, respectively.

When the optimized reactants and products are obtained, we use the multicoordinate driven (MCD) method[4] to find a low barrier reaction path that connects the reactant and product. The structure corresponding to the highest energy point in the reaction path is optimized to get the transition state. The NBO charge is also obtained for the Fe atom in the three catalysts from DFT computations.

The reaction catalyzed by Fe_2O_3 is modeled on the (001) surface, which is the most stable one. The surface model was constructed as a slab consisted of a 4 ×4 surface unit cell that were repeated under periodic boundary condition with an added vacuum layer of 20 Å. The surface was cleaved from the optimized crystal structure with the atomic layer thicknesses of 18 layers containing 122 Fe atoms and 168 O atoms. Then, the substrate is adsorbed on one Fe atom to obtain the reactant, which is optimized by DFT using the VASP5.4.1 program.[5] The first 9 layers were relaxed, while the rest were constrained in their bulk structure. Since Fe_2O_3 contains highly correlated 3*d* electrons, we chose the DFT+U formalism[6] to avoid the improper treatment of the d-

electrons by the standard DFT. The U value of 6 eV for Fe was applied. For VASP calculations, the generalized gradient approximation (GGA) in the formulation of Perdew-Burke-Ernzerhol (PBE)[7] and the projected augmented wave (PAW) method were used. In addition, DFT-D3 was invoked to account for the van der Waals interactions.[8]

When the optimized reactants and products were obtained, we used the NEB method[9] to obtain the reaction path. After optimizing the transition state, the reaction energy barrier is obtained. The Bader software was used to get the Bader charge[10] for the Fe atom in the optimized reactants and products.

Reaction Kinetics and Thermodynamics

The activation energy was calculated according to Arrhenius law:

$$k = A \times e^{-E_a/RT} \gg ln(k) = ln(A) - E_a/RT$$

The rate constant k was represented by TOF, which can be described as

$$r = TOF = k \times [acetophenone]^{\alpha} \times [benzyl\ alcohol]^{\beta},$$

The concentration of acetophenone and benzyl alcohol are regarded as constant under low conversions in the reaction (collectively named as a constant B). Therefore,

$$ln(TOF) = ln(k) + ln(B) \gg ln(TOF) = -E_a/RT + constant$$

The slope of *ln(TOF)* and *1/T* diagram is $-E_a/R$, and R is the gas constant.

Note: *TOF* was calculated from the reaction rate derived by the number of Fe atoms exposed to the catalyst surface (eqs 1 and 2):

$$TOF = n_0 c/t n_{cat} \quad (1)$$

$$n_{cat} = m_{cat}\omega/M_{Fe} \quad (2)$$

where n_0 is the initial molar of substrate, c is the conversion of substrates at the reaction of t, n_{cat} is the molar of exposed Fe atom, ω is the mass fraction of Fe in catalysts, M_{Fe} is molar mass of Fe.

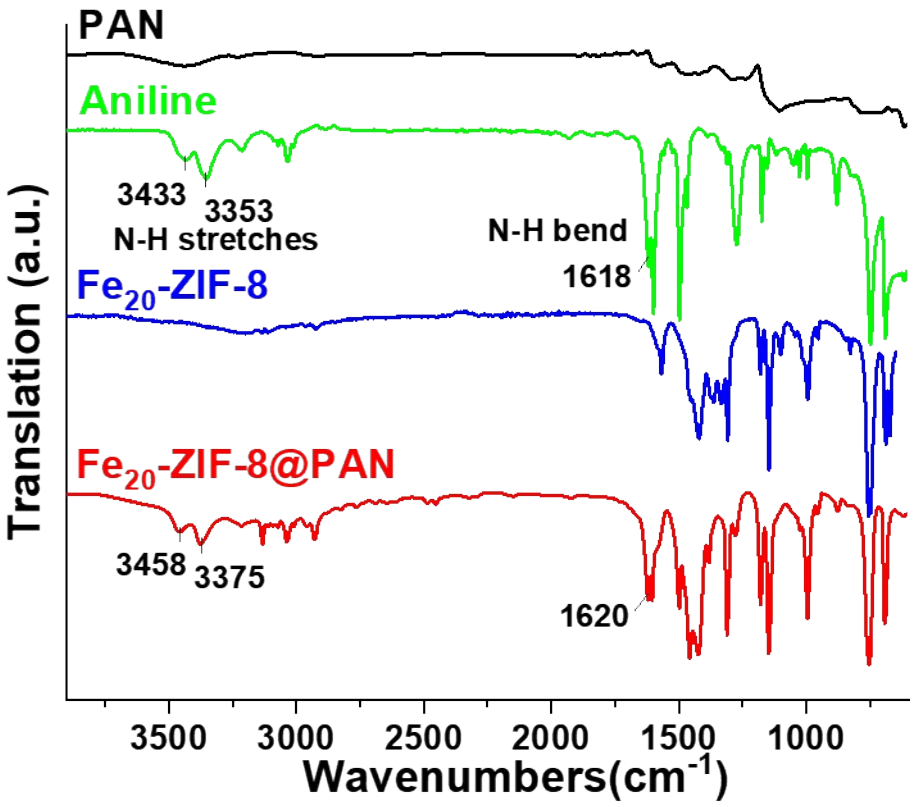

Figure S1. IR spectrum of PAN, aniline, Fe_{20}-ZIF-8 and Fe_{20}-ZIF-8@PAN

Table S1. The element content of Fe signal atom catalyst based on ICP-MS and XPS results

Catalyst	Element content (wt.%)	Characterization method
Fe_{SA}-20@NSC	2.51 (Fe)	ICP-MS
Fe_{SA}-20@NSC	79.8 (C), 4.6 (N), 12.3 (O), 2.5 (Fe), 0.8 (S)	XPS
Fe_{SA}-20@NC	2.73 (Fe)	ICP-MS

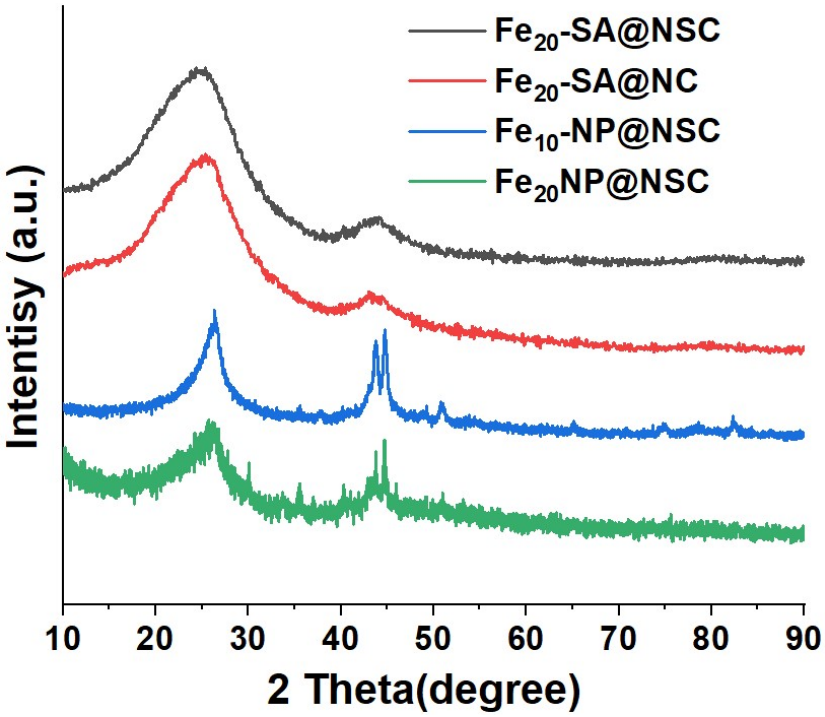

Figure S2. XRD pattern of Fe_{20}-SA@NSC, Fe_{20}-SA@NC, Fe_{10}-NP@NC and Fe_{20}NP@NSC.

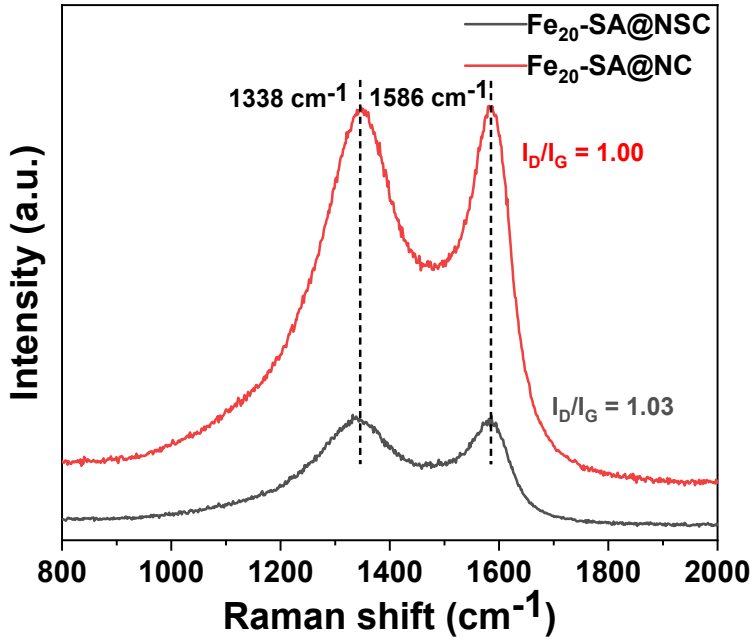

Figure S3. Raman spectra of Fe_{20}-SA@NSC and Fe_{20}-SA@NC.

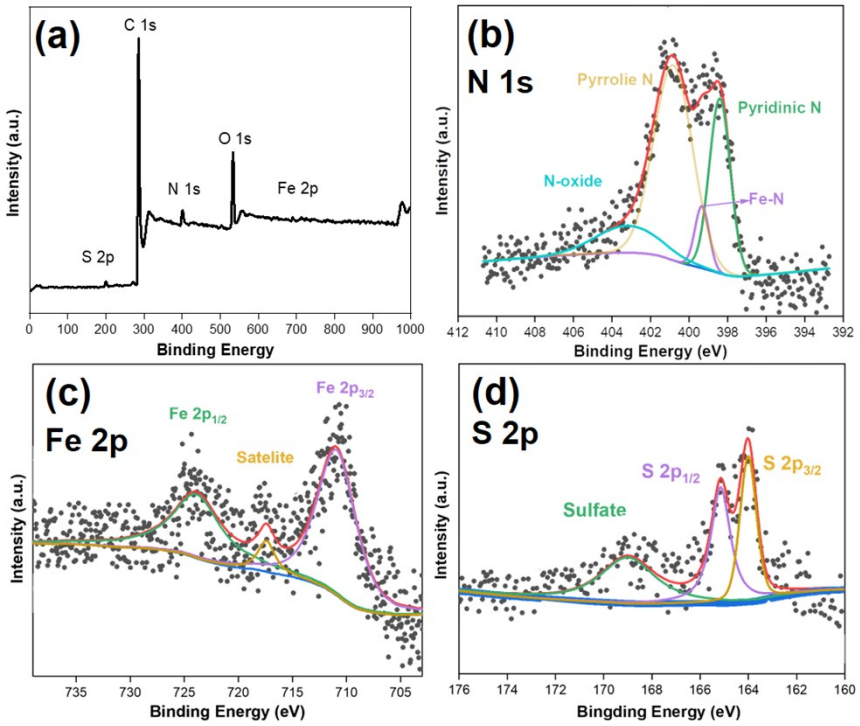

Figure S4. (a) XPS survey spectrum of Fe_{SA}-20@NSC, and the corresponding high-resolution XPS spectra of (b) N 1s, (c) Fe 2p and (d) S 2p.

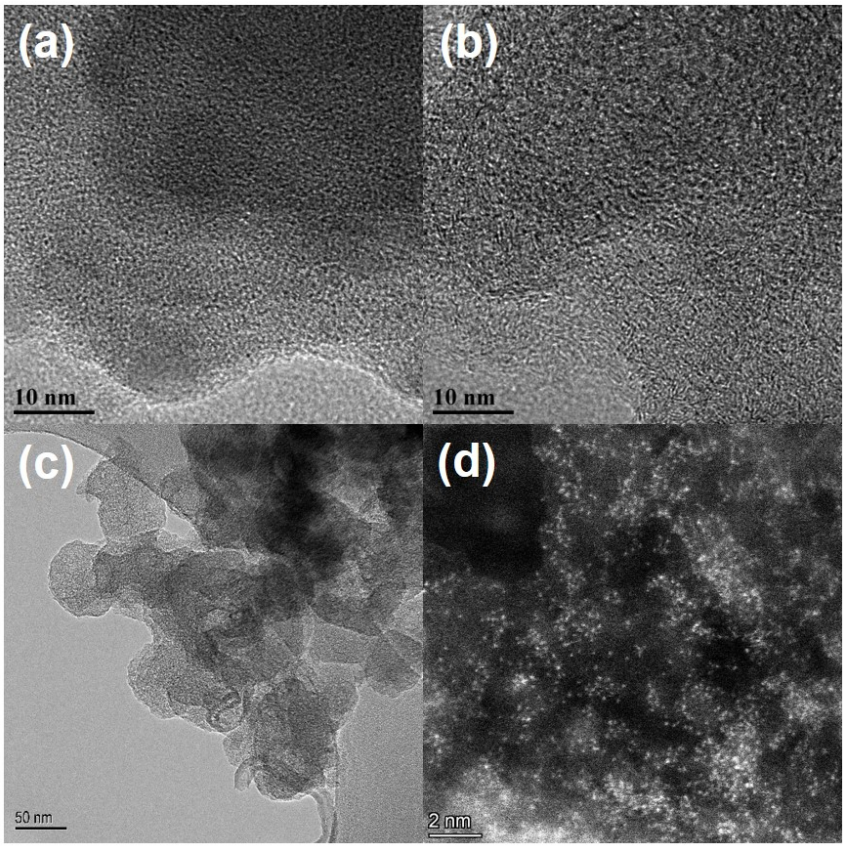

Figure S5. HRTEM images of (a) Fe_{20}-ZIF-8@PAN and (b) Fe_{20}-SA@NSC; (c) TEM and (d) HAADF-STEM image of Fe_{20}-SA@NC.

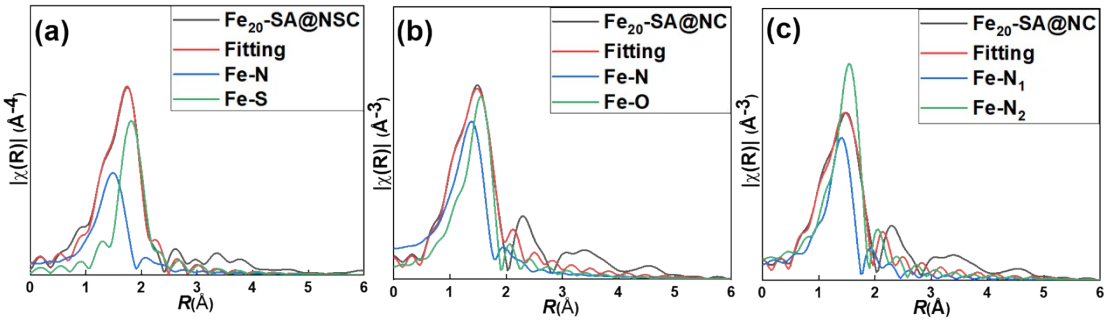

Figure S6. The Fitting of EXAFS of a) Fe_{20}-SA@NSC and (b, c) Fe_{20}-SA@NC.

Table S2. The fitting of EXAFS

Sample	Path	CN	R(Å)	$\sigma^2(10^{-3}Å^2)$	ΔE_0 (eV)	R-factor
Fe_{20}-SA@NSC	Fe-N	3.9 ± 0.2	1.97 ± 0.01	10.7 ± 0.01	-0.1 ± 0.5	0.004
	Fe-S	1.2 ± 0.1	2.24 ± 0.01	3.0 ± 0.5	1.3 ± 0.5	
Fe_{20}-SA@NC	Fe-N	3.9 ± 0.3	1.90 ± 0.05	8.0 ± 1.0	-5.8 ± 0.9	0.011
	Fe-O	2.2 ± 0.2	2.03 ± 0.09	2.5 ± 0.9		
Fe_{20}-SA@NC	$Fe-N_1$	2.3 ± 0.1	1.87 ± 0.01	2.3 ± 0.7	-4.0 ± 0.8	0.007
	$Fe-N_2$	4.2 ± 0.2	2.04 ± 0.01			

CN: coordination number; R: bonding distance; σ^2: Debye-Waller factor; ΔE_0: inner potential shift.

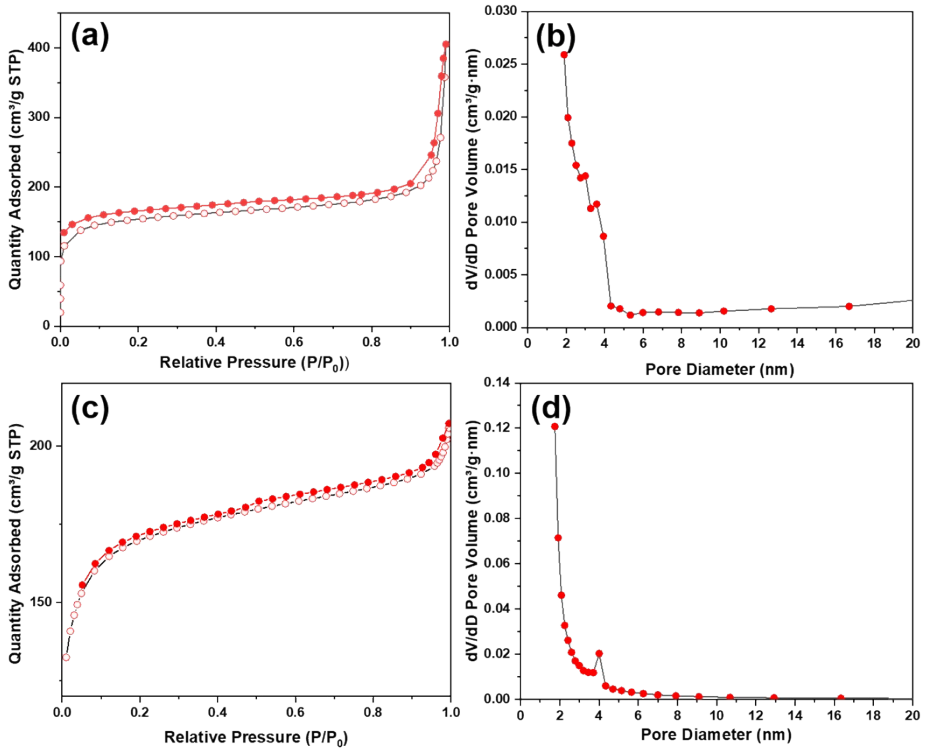

Figure S7. (a) Nitrogen adsorption–desorption isotherms and (b) the pore size distributions of Fe_{20}-SA@NSC; (c) Nitrogen adsorption-desorption isotherms and (d) the pore size distributions of Fe_{20}-SA@NC.

Table S3. The BET surface area and average pore size of Fe_{20}-SA@NSC and Fe_{20}-SA@NC

Catalyst	BET surface area (cm^3/g)	Average pore size (nm)
Fe_{20}-SA@NSC	571	2.63
Fe_{20}-SA@NC	551	2.26

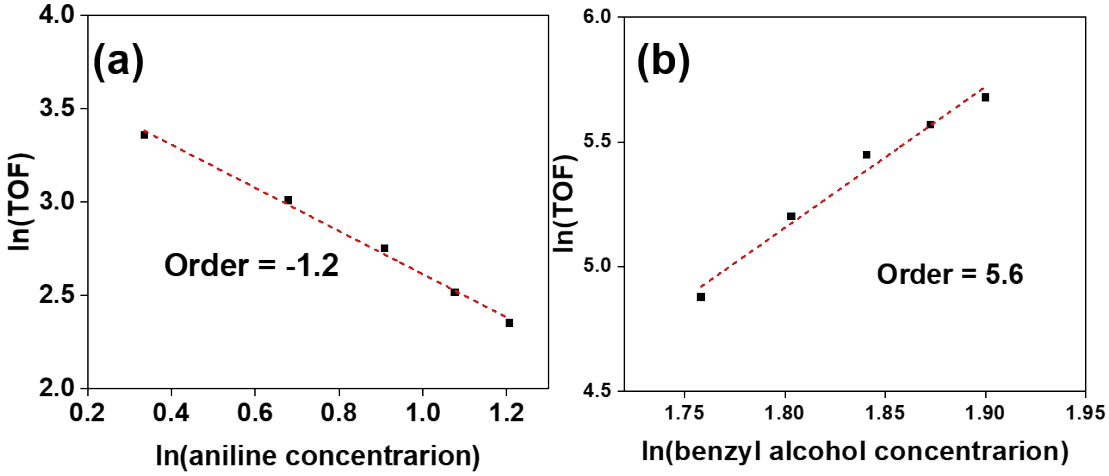

Figure S8. Plots of reaction orders for the N-alkylation of a) aniline, reaction conditions: **1a** (1 mmol, 1.5 mmol, 2 mmol, 2.5mmol, 3 mmol, respectively), **2a** (6 mmol), KOH (0.9 mmol), Fe_{20}-SA@NSC (20 mg), Ar, 135 ºC, 2 h; (b) benzyl alcohol, reaction conditions: **1a** (3 mmol), **2a** (4 mmol, 4.5 mmol, 5 mmol, 5.5 mmol, 6 mmol, respectively), KOH (0.9 mmol), Fe_{20}-SA@NSC (20 mg), Ar, 135 ºC, 2 h.

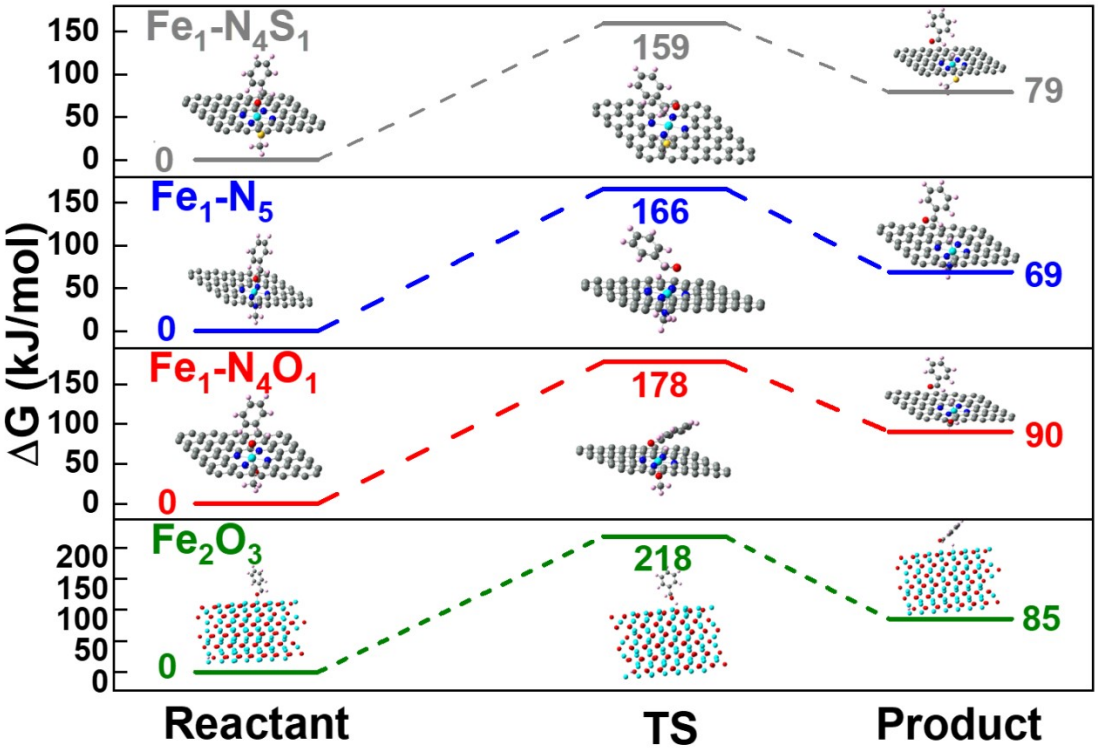

Figure S9. Partial reaction pathway and corresponding energies of Fe_1-N_4S_1, Fe_1-N_5, Fe_1-N_4O_1 and Fe_2O_3 for the N-alkylation of amines with Benzyl alcohol. Pink, black, yellow, blue, red and light blue balls represent hydrogen, carbon, sulfur, nitrogen, oxygen and iron atoms, respectively.

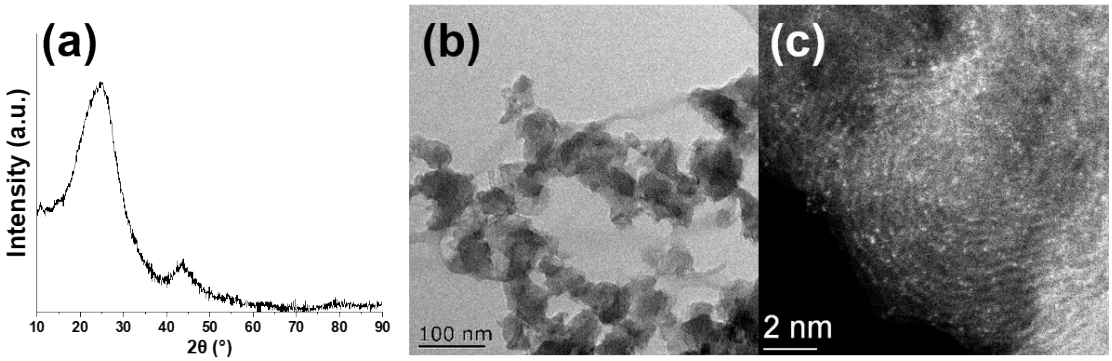

Figure S10. (a) XRD spectrum, (b) TEM and (c) HAADF-STEM images of Fe_{20}-SA@NSC after seven cycles

Reference

[1] Cosano, D.; Hidalgo-Carrillo, J.; Esquivel, D. Microwave-assisted synthesis of basic mixed oxides from hydrotalcites. J. Porous Mater. 2020, 27, 441-450.

[2] Russo, T. V.; Martin, R.L.; Hay, P.J. Effective core potentials for DFT calculations. J. Phys. Chem. 1995, 99, 17085-17087.

[3] Chiodo, S.; Russo, N.; Sicilia, E. LANL2DZ basis sets recontracted in the framework of density functional theory. J. Chem. Phys. 2006, 125, 104-107.

[4] Berente, I.; Na´ray-Szabo´, G. Multicoordinate driven method for approximating enzymatic

reaction paths: Automatic definition of the reaction coordinate using a subset of chemical coordinates. J. Phys. Chem. A. 2006, 110, 772-778.
[5] Kresse, G.; Furthmüller, J. Efficiency of ab-initio total energy calculations for metals and semiconductors using a plane-wave basis set. J. Comput. Mater. Sci. 1996, 6, 15-50.
[6] Anisimov VI; Zaanen; Andersen. Band theory and Mott insulators: Hubbard U instead of Stoner I. J. Phys. Rev. B. 1991, 44, 943-954.
[7] Perdew, J. P.; Burke, K.; Ernzerhof, M. Generalized gradient approximation made simple . Phys. Rev. Lett. 1996, 77, 3865−3868.
[8] Grimme, S. Semiempirical gga-type density functional constructed with a long-range dispersion correction. J. Comput. Chem. 2006, 27, 1787−1799.
[9] Henkelman, G; Uberuaga, BP; Jonsson, H. A climbing image nudged elastic band method for finding saddle points and minimum energy paths. J. Phys. Chem. 2000, 113, 9901-9904.
[10] Henkelman, G; Arnaldsson, A; Jonsson, H. A fast and robust algorithm for Bader decomposition of charge density. J. Comput. Mater. Sci. 2006, 36, 354-360.